Three-dimensional electromagnetic metamaterials that homogenize to uniform non-Maxwellian media

Jonghwa Shin,* Jung-Tsung Shen,† and Shanhui Fan‡
Ginzton Laboratory and Department of Electrical Engineering, Stanford University, Stanford, California 94305, USA
(Received 2 May 2007; published 14 September 2007)

We consider three-dimensional structures consisting of multiple interlocking, disconnected metal networks. We show that, in the low-frequency limit, these systems support photonic bands with linear dispersion relation. The number of such photonic bands is directly controlled by the number of networks and can be arbitrarily large. We construct a non-Maxwellian effective medium for these systems. The effective medium supports multicomponent effective fields, with the numbers of field components designable by geometry.

DOI: 10.1103/PhysRevB.76.113101 PACS number(s): 78.20.Ci, 41.20.Jb, 42.70.Qs, 78.67.Pt

Maxwell's equations describe the classical electromagnetic properties of all systems, including metamaterials, which are periodic and highly inhomogeneous. In studies of metamaterials, furthermore, one seeks to create unusual electromagnetic effects, especially in the low-frequency limit, where the wavelength in vacuum is much larger than the structural periodicity. In such a limit, it is reasonable to expect that any metamaterial can be mapped onto an effective uniform medium.[1,2] (This mapping is referred to as homogenization.[2,3]) However, most work in this area, in addition, assumes that such an effective medium itself always satisfies Maxwell's equations; i.e., the effective medium itself is Maxwellian. Hence, tremendous recent efforts have focused on discovering structures with unusual properties in electrical permittivity and magnetic permeability tensors.[4–11]

Here, we offer an alternative viewpoint by designing three-dimensional metamaterials, which may be best described by effective uniform media that is non-Maxwellian. In the low-frequency limit, these metamaterials support multicomponent effective fields, with the numbers of field components designable by geometry. Our work indicates that the physics of metamaterials is far richer than previously anticipated. In particular, new effective low-energy theory[12] with high symmetry can emerge from topological complexity alone.

We consider three-dimensional structures consisting of multiple interlocking, disconnected metal networks. Each network by itself is connected in full three dimensions. As examples, we consider three different structures with two, five, and four networks, respectively (Figs. 1–3). These structures all possess a cubic unit cell and either a cubic (Figs. 1 and 2) or pyritohedral (Fig. 3) point group.[13]

We calculate the dispersion relation of these structures using finite difference time domain methods, which solve the underlying Maxwell's equations from first principles with no uncontrolled approximation. The computational domain corresponds to one cubic unit cell with Bloch-periodic boundary conditions,[14] discretized with 48 grid points in each direction. The simulations yield a band structure assuming a cubic unit cell. Since the cubic unit cell contains all networks, the results thus obtained can be directly compared to the effective field theory.

The simulations reveal that in the low-frequency limit, the structures in Figs. 1–3 support one, four, and three bands with linear dispersion relations, respectively [Figs. 1(b), 2(b), and 3(b)]. (The nondegenerate nature of the band for the structure in Fig. 1 is further confirmed by examining the corresponding field pattern of the mode, which has the full symmetry of the lattice [inset of Fig. 1(b)].) In these systems, the number of low-frequency bands is directly controlled by the number of networks and can be arbitrarily large. Therefore, these dispersion relations differ from *all* metamaterials previously considered.

We construct an effective medium that is local and non-Maxwellian for these structures. Our approach, which is quasistatic,[15] is exact in the low-frequency limit. The electro- and magnetostatic properties of any N-network system is described as

$$\mathbf{Q} = \mathbf{C}\mathbf{V},$$

$$\mathbf{A} = \mathbf{L}\mathbf{I}. \tag{1}$$

Here, $\mathbf{V}$ and $\mathbf{Q}$ are N-vectors. Their components, $\mathbf{V}_i$ and $\mathbf{Q}_i$, are the voltage and the charge density (averaged over the unit cell volume), respectively, of the ith network. $\mathbf{A}$ and $\mathbf{I}$ are $3N$-vectors. $\mathbf{I}_{iu}$ is the total current through a unit cell surface normal to the u direction divided by the area of the surface ($u \in \{x,y,z\}$). $\mathbf{A}_{iu}$ is a line average of the microscopic vector potential $\vec{A}$,

$$\mathbf{A}_{iu} = a^{-1} \int_{\vec{r}_i}^{\vec{r}_i + a\hat{u}} \vec{A} \cdot d\vec{l}, \tag{2}$$

where a is the unit cell length, and the integration path remains on the ith network. $\mathbf{C}$ and $\mathbf{L}$ are the capacitance and inductance matrices.

For time-varying fields, the microscopic electric field still vanishes inside a perfect conductor, i.e., $\vec{E} = -\nabla V - \partial \vec{A}/\partial t = 0$. Integrating this relation, along the same path as in Eq. (2), results in

$$\nabla \mathbf{V} = -\frac{\partial \mathbf{A}}{\partial t}. \tag{3}$$

Also, the microscopic current density and charge density are related by $\nabla \cdot \vec{J} = -\partial \rho / \partial t$. Again, by averaging, we have

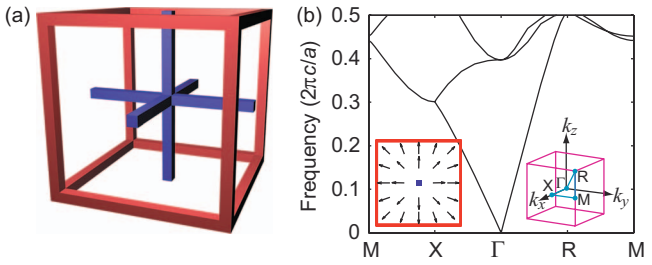

FIG. 1. (Color) Two-network structure. (a) A single cubic unit cell of the structure is depicted. Each network, represented by different colors, consists of wires along the edges of a cube. The two networks are displaced from one another by $\sqrt{3}a/2$ along the [111] direction. (b) The band diagram is shown along high-symmetry k points. The right inset shows the high-symmetry points in the first Brillouin zone. The left inset shows the electric field profile on the $z=0$ plane, for a mode at $\omega=0.033(2\pi c/a)$, with its wave vector along the [001] direction. Here, c is the speed of light in vacuum.

$$\nabla \cdot \mathbf{I} = -\partial \mathbf{Q}/\partial t. \tag{4}$$

Equations (3) and (4) are exact and are not restricted to the quasistatic limit.

In the quasistatic limit, the dynamic variables, **V**, **Q**, **I**, and **A**, vary at a length scale much longer than the periodicity. Thus, within each unit cell, Eq. (1) remains valid. Combining this with Eqs. (3) and (4) leads to the equation for **V**,

$$\frac{\partial^2 \mathbf{V}}{\partial t^2} = \mathbf{C}^{-1} \nabla \cdot (\mathbf{L}^{-1} \nabla \mathbf{V}). \tag{5}$$

In deriving Eq. (5), we note that the capacitance matrix **C** has a zero eigenvalue, since a constant shift in the voltages of all networks does not modify charge distributions or field profiles in the infinitely periodic structure. Also, three of the eigenvalues of the inductance matrix **L** are infinite, since a nonzero total current in the same direction in every unit cell results in infinite vector potential. However, wave solutions have zero total voltage and current in each unit cell, i.e., $\Sigma_i \mathbf{V}_i = 0$ and $\Sigma_i \mathbf{I}_{iu} = 0$. Thus, in Eq. (5) $\mathbf{C}^{-1}$ and $\mathbf{L}^{-1}$ can be properly defined with nonsingular eigenvalues, within the subspace of wave solutions, by first projecting out the eigenvectors associated with the zero or infinite eigenvalues of **C**

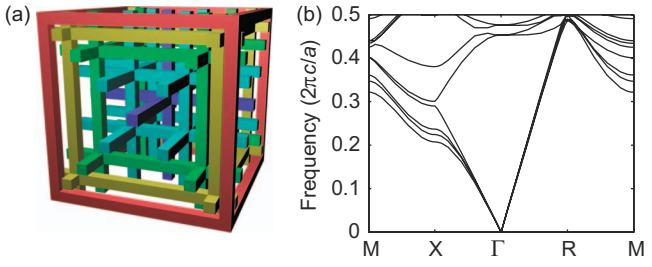

FIG. 2. (Color) N-network cubic structure, where N can be arbitrarily large. Each network has metal wires along the x, y, and z directions. For the ith network, these wires meet at $(\pm x_i, \pm x_i, \pm x_i)$ in the cubic unit cell. Shown here is a five network example with x_i's chosen to be 0, $a/12$, $3a/16$, $a/3$, and $a/2$: (a) the unit cell and (b) the band diagram.

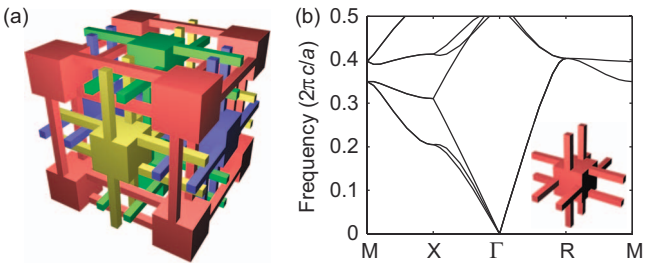

FIG. 3. (Color) Four-network fcc structure. (a) Unit cell; (b) band diagram. Each network [inset of (b)] is identical in shape and is made by translating x-, y-, and z-directional wires on the edges of a cube by $\pm(a/8)\hat{y}$, $\pm(a/8)\hat{z}$, and $\pm(a/8)\hat{x}$, respectively. These wires are then connected by a small cube at each site of a face-centered-cubic (fcc) lattice. The basis element is topologically identical to Borromean rings (Ref. 29).

and **L**. To emphasize this, below, we refer to $\mathbf{C}^{-1}$ and $\mathbf{L}^{-1}$ as **S** and **U**, respectively.

Equation (5) describes the dynamics of an effective field **V** with $N-1$ independent components in an effective uniform medium characterized by the matrices **S** and **U**. Since **S** and **U** have no wave vector dependency, the theory is local. The components of **V** represent the internal degrees of freedom of the effective field. They are analogous to polarization for Maxwellian fields. However, unlike polarizations, these internal degrees of freedom are designable by geometry and hence can exhibit much richer behaviors. Below, we will use the theory [Eq. (5)] to account for the details of the simulation results shown in Figs. 1–3.

Case (1): Two-network crystal. For the structure in Fig. 1 (the dc conductivity behavior of such a two conductor geometry has been studied, for example, in Ref. 16), the effective field **V** has only one degree of freedom and the **S** matrix has a form of

$$S_{12}\begin{pmatrix} -1 & 1 \\ 1 & -1 \end{pmatrix}.$$

Since each network has fourfold rotational symmetry axes along the x, y, and z directions that pass through the origin, it

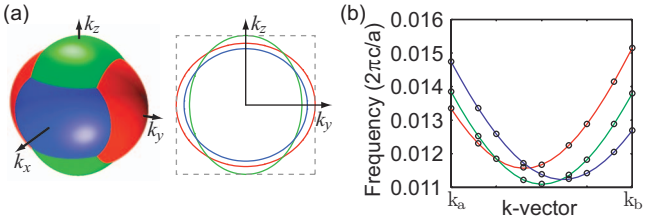

FIG. 4. (Color) Detailed comparison of theory and simulations for the four-network fcc system shown in Fig. 3. (a) Isofrequency surfaces and contours of three low-frequency modes. The plot on the right shows the contour on the $k_x=0$ plane. Gray dashed lines represent a square tangential to some of the contours. (b) Frequencies of modes for k-vectors along a $\mathbf{k}_a - \mathbf{k}_b$ line segment, where $\mathbf{k}_a = (2\pi/a)$ (0.0025, 0.016, 0.0175) and $\mathbf{k}_b = (2\pi/a)$ (0.0225, 0, 0.0075). The lines are theory predictions and the circles are finite difference time domain results. These k points are arbitrarily chosen. The agreement between theory and simulation is, in fact, excellent for all k points.

can be proved that $U_{iu,jv}=U_{ij}\delta_{uv}$. Therefore, $\mathbf{U}$ matrix is isotropic with respect to propagation direction, and Eq. (5) predicts that the structure has a single low-frequency mode with isotropic dispersion relation, consistent with simulations.

The two-network system thus supports an isotropic scalar effective field. In using optical waves for communication, polarization dependency due to the vector nature of electromagnetic fields is a major detriment. In connection with the use of novel fiber structures to create scalar field in one dimension,[17] our work suggests a route toward completely erasing polarization dependency in all three dimensions. In particular, the field profile in a unit cell closely matches that of those novel fiber structures.

Case (2): N-network cubic crystal. For the structure in Fig. 2, since all networks share the same symmetry axes for fourfold rotation, $U_{iu,jv}=U_{ij}\delta_{uv}$ still holds, and the band structure for this case of Fig. 2 is isotropic. However, these modes are, in general, nondegenerate in spite of the cubic symmetry of the structure. For the five-network structure shown here, simulation indeed observes four nondegenerate low-frequency bands.

In such structures, the number of bands in the low-frequency regime is $N-1$. Hence, the density of states can be greatly enhanced over very broad bandwidth when N is large. This may have important consequences for radiation and spontaneous emission control. In contrast, previous attempts to control spontaneous emission involve either broadband suppression using photonic band gap[18] or narrow-band enhancement using microcavities.[19] Also, with nonlinear materials introduced between the metal regions, these structures may provide an experimental system to study interaction properties of N-component fields, which is of interest in modern field theory but until now has largely remained a theoretical novelty.[20] Finally, the three-network systems, with two low-frequency modes, can be designed to function as a transparent electrode that is important for light emitting diodes and photovoltaic applications. In particular, by placing arrays of dipole antennas at the surface of the structure, where the arms of the antennas are connected to different networks, the coupling between external plane waves and the internal modes can reach 100%.[21]

Case (3): Four-network fcc crystal. The structure in Fig. 3 has a pyritohedral (T_h) symmetry and an fcc lattice. Based on the symmetries, the $\mathbf{S}$ and $\mathbf{U}$ matrices become

$$\mathbf{S}=S_{12}\begin{pmatrix}-3 & 1 & 1 & 1\\ 1 & -3 & 1 & 1\\ 1 & 1 & -3 & 1\\ 1 & 1 & 1 & -3\end{pmatrix},$$

$$\mathbf{U}=\begin{pmatrix}\mathbf{U}_{11} & \mathbf{U}_{12} & \mathbf{U}_{13} & \mathbf{U}_{14}\\ \mathbf{U}_{12} & \mathbf{U}_{11} & \mathbf{U}_{14} & \mathbf{U}_{13}\\ \mathbf{U}_{13} & \mathbf{U}_{14} & \mathbf{U}_{11} & \mathbf{U}_{12}\\ \mathbf{U}_{14} & \mathbf{U}_{13} & \mathbf{U}_{12} & \mathbf{U}_{11}\end{pmatrix},$$

$$\mathbf{U}_{12}=\begin{pmatrix}U_{1x,2x} & 0 & 0\\ 0 & U_{1y,2y} & 0\\ 0 & 0 & U_{1z,2z}\end{pmatrix},$$

$$\mathbf{U}_{13}=\begin{pmatrix}U_{1z,2z} & 0 & 0\\ 0 & U_{1x,2x} & 0\\ 0 & 0 & U_{1y,2y}\end{pmatrix},$$

$$\mathbf{U}_{14}=\begin{pmatrix}U_{1y,2y} & 0 & 0\\ 0 & U_{1z,2z} & 0\\ 0 & 0 & U_{1x,2x}\end{pmatrix},$$

$$\mathbf{U}_{11}=-(\mathbf{U}_{12}+\mathbf{U}_{13}+\mathbf{U}_{14}). \tag{6}$$

The isofrequency surfaces in k space for the three modes are the three separate ellipsoids related by rotation, having the major axis in the x, y, and z directions, respectively [Fig. 4(a)]. These ellipsoids intersect at the [111] direction where the three modes become degenerate.

The band structure of this system is controlled by three parameters $S_{12}U_{1x,2x}$, $S_{12}U_{1y,2y}$, and $S_{12}U_{1z,2z}$. These parameters can be directly obtained from electrostatic and magnetostatic solutions. Alternatively, these can also be numerically determined by calculating the frequencies of the three modes at a single k point [e.g., $(0,0,0.04\pi/a)$] where the modes are nondegenerate. The full dispersion relation along all directions can then be obtained using Eq. (5) and compared to simulations. The excellent agreements between theory and simulations [Fig. 4(b)] provide a strong validation of our effective field approach.

Finally, we note that the most general Maxwellian medium has the following constituent relation of a bianisotropic form:[22]

$$\vec{D}=\varepsilon\vec{E}+\alpha\vec{H},$$

$$\vec{B}=\beta\vec{E}+\mu\vec{H}, \tag{7}$$

where $\vec{D}$, $\vec{B}$, $\vec{E}$, and $\vec{H}$ are the electric and magnetic flux densities and electric and magnetic fields, respectively. ε and μ are the electric permittivity and magnetic permeability tensors, and α and β are the tensors that describe magnetoelectric effects. If none of the constituent tensors depend on the wave vector $\vec{k}$, the medium is defined as local. (Our definition here of a local Maxwellian medium is slightly more general than typically used. In many published papers, the magnetoelectric effect is instead incorporated as a first-order nonlocal contribution to ε and μ, and a medium having magnetoelectric effect is therefore sometimes referred to as a nonlocal medium.[22,23] This difference in definition has no consequence in our subsequent discussions.)

For a local Maxwellian medium with the same spatial symmetry as the structures shown in Figs. 1–3, one can prove that $\alpha=\beta=0$ and both ε and μ are scalar.[22,23] Hence, the medium supports either zero[4] or two[14] photonic bands at the limit $\omega\to 0$, depending on the sign of $\varepsilon(\omega)\mu(\omega)$. In the latter case, the bands are doubly degenerate and isotropic, i.e., $\omega=\omega(|\vec{k}|)$ and the isofrequency surface is spherical.[14] In contrast, the numbers of bands in the low-frequency limit, as well as their detailed modal properties, prove that the structures in Figs. 1–3 cannot homogenize to any local Maxwellian medium.

It is certainly interesting to try to homogenize these structures to a nonlocal Maxwellian medium. Many metamaterials can be homogenized to Maxwellian media that exhibit strong nonlocal effects in the low-frequency limit.[24–28] However, the standard homogenization approaches[2,23] assume the existence of macroscopic electromagnetic fields that are uniform over the length scale of a unit cell. These approaches are difficult to apply here because the averaging processes in these approaches fundamentally remove all physics related to the spatial variations of the fields at small length scales, and hence tend to produce zero macroscopic fields for our structures. Instead, our local non-Maxwellian theory is appealing: With the information about field variations at small length scales captured as the internal degrees of freedom of the effective fields, our theory directly highlights the unusual symmetry properties that emerge from topological complexities.

This work is supported in part by ARO (Grant No. DAAD-19-03-1-0227), AFOSR (Grant No. FA9550-04-1-0437), NSF (Grant No. ECS-0134607), and a Samsung Scholarship.

*jshin@jshin.info
†jushen@gmail.com
‡shanhui@stanford.edu

[1] D. R. Smith, J. B. Pendry, and M. C. K. Wiltshire, Science **305**, 788 (2004).
[2] D. R. Smith and J. B. Pendry, J. Opt. Soc. Am. B **23**, 391 (2006).
[3] G. W. Milton, *The Theory of Composites* (Cambridge University, Cambridge, 2001).
[4] J. B. Pendry, A. J. Holden, W. J. Stewart, and I. Youngs, Phys. Rev. Lett. **76**, 4773 (1996).
[5] D. F. Sievenpiper, E. Yablonovitch, J. N. Winn, S. Fan, P. R. Villeneuve, and J. D. Joannopoulos, Phys. Rev. Lett. **80**, 2829 (1998).
[6] J. B. Pendry, A. J. Holden, D. J. Robbins, and W. J. Stewart, IEEE Trans. Microwave Theory Tech. **47**, 2075 (1999).
[7] G. V. Eleftheriades, A. K. Iyer, and P. C. Kremer, IEEE Trans. Microwave Theory Tech. **50**, 2702 (2002).
[8] D. R. Smith and D. Schurig, Phys. Rev. Lett. **90**, 077405 (2003).
[9] N. Engheta and R. W. Ziolkowski, IEEE Trans. Microwave Theory Tech. **53**, 1535 (2005).
[10] J. T. Shen, P. B. Catrysse, and S. Fan, Phys. Rev. Lett. **94**, 197401 (2005).
[11] V. M. Shalaev, Nat. Photonics **1**, 41 (2007).
[12] P. W. Anderson, Science **177**, 393 (1972).
[13] M. Hamermesh, *Group Theory and Its Application to Physical Problems* (Dover, New York, 1989).
[14] S. Fan, P. R. Villeneuve, and J. D. Joannopoulos, Phys. Rev. B **54**, 11245 (1996).
[15] U. S. Inan and A. S. Inan, *Engineering Electromagnetics* (Prentice Hall, Upper Saddle River, NJ, 1998), Chaps. 2 and 3.
[16] M. Briane and L. Mazliak, Port. Math. **55**, 187 (1998).
[17] M. Ibanescu, Y. Fink, S. Fan, E. L. Thomas, and J. D. Joannopoulos, Science **289**, 415 (2000).
[18] E. Yablonovitch, Phys. Rev. Lett. **58**, 2059 (1987).
[19] Y. Yamamoto and R. E. Slusher, Phys. Today **46**(6), 66 (1993).
[20] A. Zee, *Quantum Field Theory in a Nutshell* (Princeton University, Princeton, NJ, 2003).
[21] J. Shin, J. T. Shen, and S. Fan (unpublished).
[22] V. M. Agranovich and V. L. Ginzburg, *Crystal Optics with Spatial Dispersion and Excitons* (Springer-Verlag, Berlin, 1984).
[23] P. Halevi and F. Perez-Rodriguez, Proc. SPIE **6320**, 63200T (2006).
[24] A. L. Pokrovsky and A. L. Efros, Phys. Rev. B **65**, 045110 (2002).
[25] P. A. Belov, R. Marqués, S. I. Maslovski, I. S. Nefedov, M. Silveirinha, C. R. Simovski, and S. A. Tretyakov, Phys. Rev. B **67**, 113103 (2003).
[26] M. G. Silveirinha and C. A. Fernandes, IEEE Trans. Microwave Theory Tech. **52**, 889 (2004).
[27] C. R. Simovski and P. A. Belov, Phys. Rev. E **70**, 046616 (2004).
[28] M. A. Shapiro, G. Shvets, J. R. Sirigiri, and R. J. Temkin, Opt. Lett. **31**, 2051 (2006).
[29] P. R. Cromwell, E. Beltrami, and M. Rampichini, Math. Intell. **20**(1), 53 (1998).